

www.acsnano.org

One-Dimensional van der Waals Heterojunction Diode

Ya Feng,* Henan Li, Taiki Inoue, Shohei Chiashi, Slava V. Rotkin, Rong Xiang, and Shigeo Maruyama*



Cite This: ACS Nano 2021, 15, 5600-5609



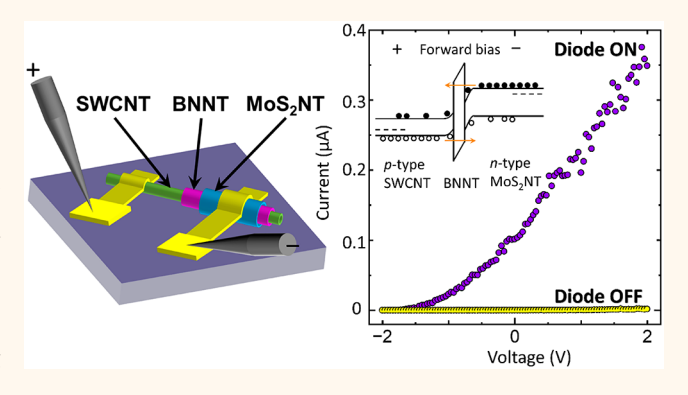
ACCESS I

Metrics & More

Article Recommendations

s Supporting Information

ABSTRACT: The synthesis of one-dimensional van der Waals heterostructures was realized recently, which offers alternative possibilities for prospective applications in electronics and optoelectronics. The even reduced dimension will enable different properties and further miniaturization beyond the capabilities of their two-dimensional counterparts. The natural doping results in *p*-type electrical characteristics for semiconducting single-walled carbon nanotubes and *n*-type for molybdenum disulfide with conventional noble metal contacts. Therefore, we demonstrate here a one-dimensional heterostructure nanotube, 11 nm wide, with the coaxial assembly of a semiconducting single-walled carbon nanotube, insulating boron nitride nanotube, and semiconducting molybdenum



disulfide nanotube, which induces a radial semiconductor—insulator—semiconductor heterojunction. When opposite potential polarity was applied on a semiconducting single-walled carbon nanotube and molybdenum disulfide nanotube, respectively, the rectifying effect was materialized.

KEYWORDS: single-walled carbon nanotubes, one-dimensional heterostructure, heterojunction diode, boron nitride nanotubes, molybdenum disulfide, van der Waals

 \mathbf{y} emiconductor p-n junctions are fundamental to build up state-of-the-art optoelectronic architectures. The emerging two-dimensional (2D) van der Waals assemblies, 2,3 including atomically thin semiconducting transition metal dichalcogenides (TMDs) and engineered graphene, have pushed p-n junctions to an ultimate thickness limit, which enable tunneling diodes with a negative differential resistance (NDR),⁴ tunneling transistors,^{5,6} unusual photovoltaic devices,^{7,8} and quantum well light-emitting diodes (LEDs).9 With further dimension confining, the rolled-up graphene one-dimensional (1D) single-walled carbon nanotube (SWCNT) can induce a direct bandgap, therefore allowing various applications in optoelectronics. ^{10–13} Efforts have been made to realize a single SWCNT diode through chemical doping, 14,15 which suffers from short durability, by introducing asymmetric metal contacts, 16 which involve multiple intricate metal deposition processes, or via electrostatic doping, 17,18 which, however, is limited by the gate leakage and also requires processing with multiple metals 19 in order to generate a built-in potential to drive flow of carriers unidirectionally.

The considerable performance improvement of 2D electronic devices by van der Waals layer stacking^{20,21} as well as the versatilities it presents^{4,9} have intrigued the exploration of

van der Waals heterostructures in a 1D field, and such 1D counterpart templating with SWCNT has been synthesized by chemical vapor deposition (CVD) recently.²² Therefore, a 1D ultrathin heterojunction can be expected from a naturally *p*-doped semiconducting SWCNT²³ and an *n*-doped molybdenum disulfide nanotube (MoS₂NT)²⁴ heterostructure. In the present work, we propose a radial semiconductor—insulator—semiconductor (S—I—S) heterojunction with a 1D heterostructure composed of a coaxial SWCNT, boron nitride nanotube (BNNT), and MoS₂NT. In contrast to lateral 1D devices that suffer from fringe fields and incomplete electrostatic gating, radial (wrap-around) geometry gives the ultimate control of 1D charge density.^{25,26} We synthesized micrometerlong SWCNT bridging over silicon poles and then coated it with a BNNT to increase the diameter in order to complete the ultimate coating of MoS₂NT. This 1D S—I—S heterojunction results in a significant rectifying effect with one

Received: January 24, 2021 Accepted: February 23, 2021 Published: March 1, 2021





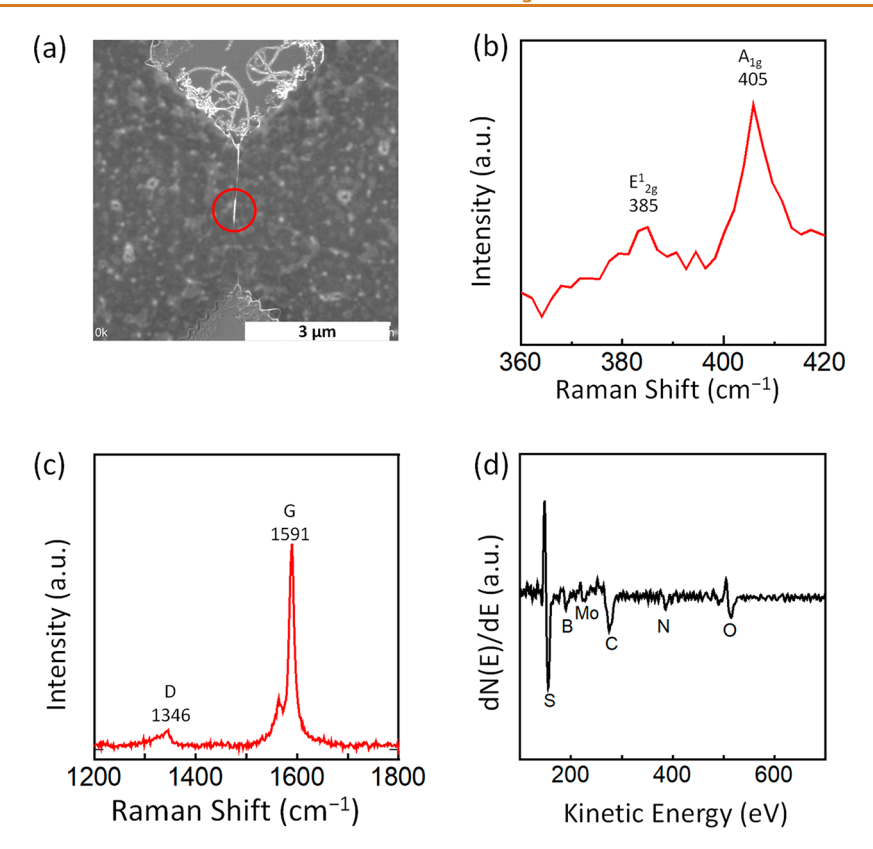


Figure 1. Characterizations of the suspended SWCNT/BNNT/MoS₂NT heterostructure nanotube. (a) SEM image of the suspended nanotube. Raman spectrum (the laser spot was focused on the red-circle area in (a)) shows the fingerprint peaks from MoS_2 in (b) as well as D and G peaks from the SWCNT in (c). (d) AES spectrum from the suspended nanotube area.

electrode touching the inner semiconducting SWCNT while the other is in contact with the outmost MoS_2NT . The 1D S–I–S heterojunction diode presented in this work as scalable as single-molecule diodes^{27,28} can readily fit into the current semiconducting industry, providing an alternative method to further miniaturize optoelectronic building blocks. The feasibility shown by the current 1D heterojunction diode and the multifunctionalities inherent in the heterostructure imply the tremendous potential in near-future electronic and optoelectronic applications.

RESULTS AND DISCUSSION

The micrometer-long suspended SWCNT was prepared over Si poles with confined Co catalysts on the top as illustrated in Figure S1. The small patterned catalyst areas effectively avoided SWCNT bundles during growth. Thereafter, BNNT and MoS2NT coating were sequentially conducted. More detailed growth preparations can be found in Figure S2. Nonuniformities accumulated along suspended nanotubes after BNNT coating because of the rather randomly distributed nucleation sites. Further MoS₂NT coating along the suspended nanotube presents sharp contrasts as shown in the scanning electron microscope (SEM) images of Figure S3. A confocal Raman spectrum with a laser wavelength of 532 nm focusing on the red-circle site in Figure 1(a), which is seemingly thicker and brighter under SEM, exhibits the fingerprint peaks of molybdenum disulfide (MoS₂) located at 385 and 405 cm⁻¹ Raman shifts in Figure 1(b), respectively, as well as D and G peaks from the SWCNT shown in Figure 1(c). The weak nonresonant boron nitride (BN) Raman scattering that overlaps with the D peak of CNT²⁹ is unable to manifest here. The full spectrum including the radial breathing mode (RBM) from SWCNT as well as arrow-marked peaks from the substrate are presented in Figure S4. Auger electron spectroscopy (AES) was employed to verify the composition of the suspended heterostructure nanotube. Figure 1(d) demonstrates an AES spectrum from an as-grown heterostructure nanotube with an excitation electron beam of 10 kV and 10 nA, which detected carbon, boron, nitrogen, molybdenum, and sulfur atoms from the suspended nanotube as shown in Figure 1(a), where oxygen is originated from environmental adsorption or substrate. From the above analysis, we can draw a conclusion that the relatively brighter parts in SEM images surfaced after the second and third CVD processes on the suspended heterostructure nanotube can be attributed to the successful coating of BNNT and/or MoS2NT van der Waals layers.

The prepared 1D heterostructures were then face-transferred, taking advantage of a water vapor assisting technique, onto the target chip, and a schematic illustration about this process is presented in Figure S5. The SEM images captured after wet transfer present obvious contrasts from some nanotubes but are absent from some others as compared in Figure S6. As characterization results revealed in Figure 1, the thick and bright parts were successfully covered by BNNT and/or MoS₂NT, so we could roughly identify heterogeneous parts on a specific post-transferred nanotube by SEM and design the metal contacts accordingly to fabricate a possible S–I–S heterojunction diode. A scattering-type scanning nearfield optical microscope (s-SNOM) has been utilized to explore hexagonal boron nitride (hBN). 31–33 s-SNOM allows the optical material signatures to be detected with the highest

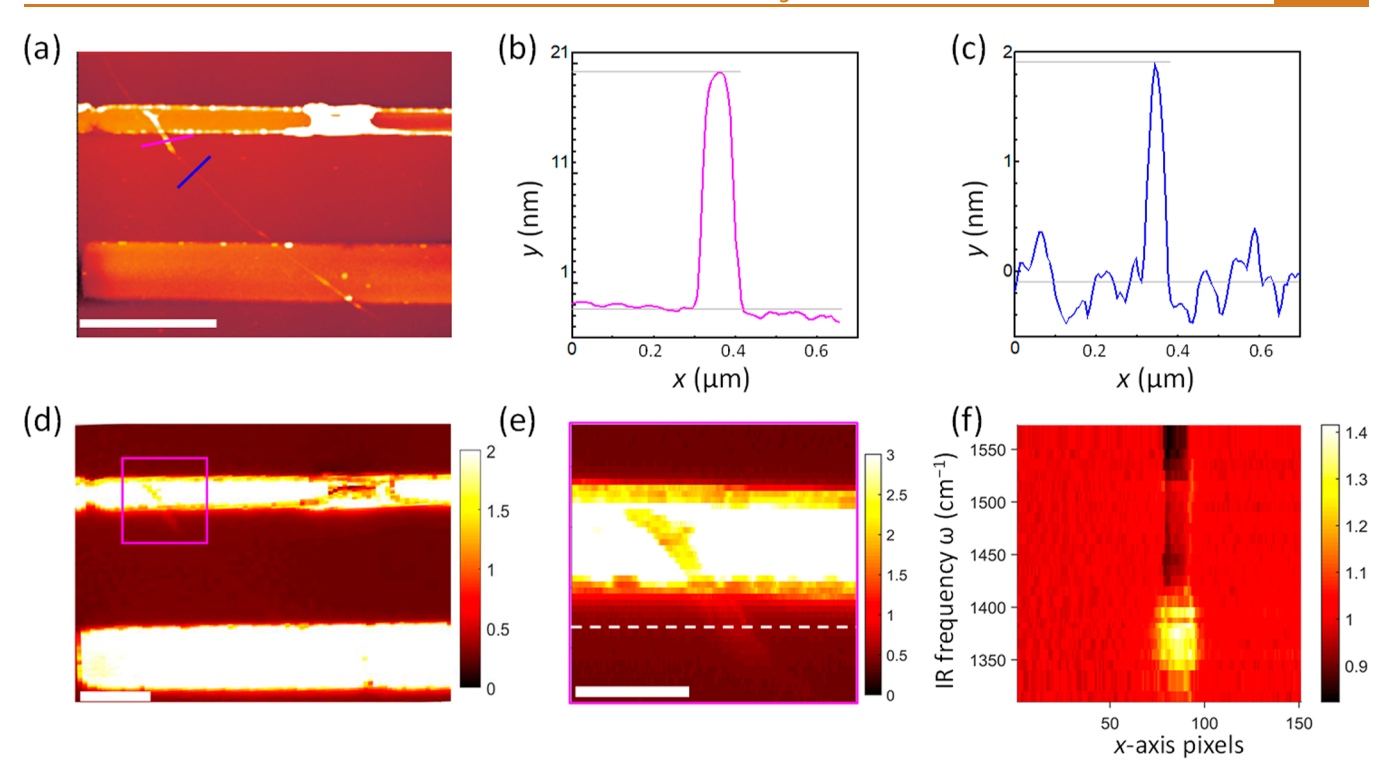


Figure 2. (a) AFM topography image of the heterostructure nanotube. Height profiles show that (b) the thick part of the nanotube (purple line in (a)) is about 20 nm, while (c) the thin part (blue line in (a)) is around 2 nm. (d) s-SNOM S₂-amplitude image of a heterostructure nanotube at IR frequency $\omega = 1350 \text{ cm}^{-1}$; the thick part in purple square area is enlarged in (e). (f) s-SNOM hyperspectral cross section: profiles taken along the dashed white line in (e) and normalized to the background, from scans at IR frequencies of $1310 \sim 1573 \text{ cm}^{-1}$. Scale bars: (a) 2 μ m, (d) 1 μ m, and (e) 400 nm.

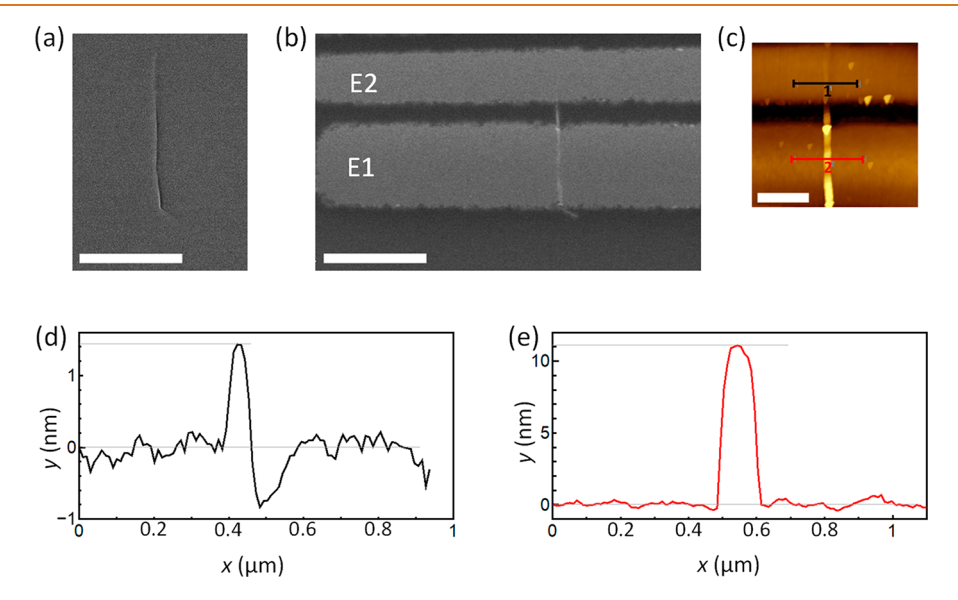


Figure 3. SEM images of the 1D heterostructure (a) before and (b) after metal contact deposition. (c) AFM mapping of (b) and the profiles 1 and 2 are shown in (d) and (e), respectively. Scale bars: (a) 1 μ m, (b) 1 μ m, and (c) 500 nm.

spatial resolution, limited only by its tip radius and signal-tonoise ratio. Here, we resolved the 2 nm thin heterostructure nanotube, smeared in a wider pattern by the instrumental tip function in Figure 2, which was because of a high optical contrast achieved when tuning the excitation laser to a peculiarly strong phonon resonance of hBN. Figure 2(d) shows the s-SNOM map of one device along with the thick part of the heterostructure nanotube enlarged in Figure 2(e) at an infrared (IR) frequency $\omega = 1350$ cm⁻¹. The images were collected in pseudoheterodyne (PsHet) mode of a Neaspec s-SNOM (tapping amplitude ≈ 70 nm, ARROW-NCPt tips by Nanoworld < 25 nm radius, excitation by quantum cascade laser MIRCat by Daylight in CW mode at power < 2 mW in focal aperture), tuned to show a strong s-SNOM signal in all PsHet harmonics S_1-S_4 . S_2 was used for Figures 2 and S_7 , where a sequence of images at 26 different frequencies is shown, constituting a hyperspectral cube: $S_2(f, x, y)$ for amplitude vs. frequency and two spatial coordinates. Taking a

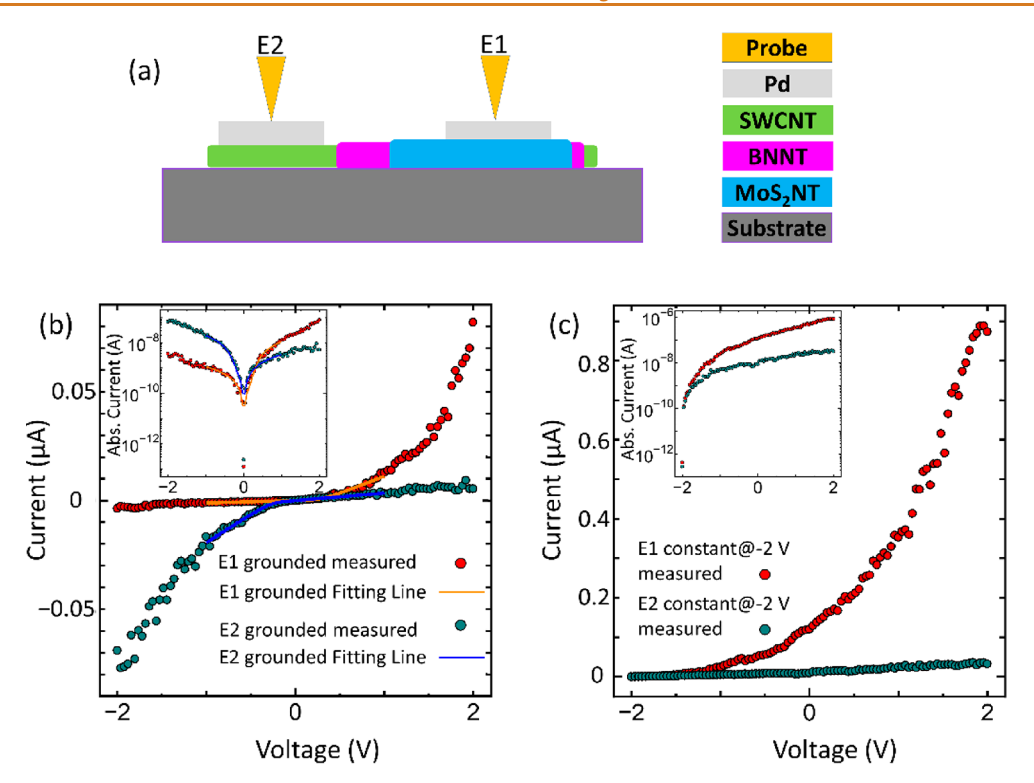


Figure 4. (a) Schematic cross-sectional view of the measured 1D heterojunction diode. (b) Electrical characteristics: the red dots are measured when electrode E1 (denoted in the schematic and SEM image of Figure 3(b)) is grounded while electrode E2 is sweeping from -2 to 2 V, and the orange solid line is the fitting for experimental data; the olive dots are from the reverse situation, and the blue solid line is the fitting for experimental data. The inset shows the same curves in the semilogarithmic axis. (c) Electrical characteristics: the red dots are measured when electrode E1 is applied with a constant voltage of -2 V while electrode E2 is sweeping from -2 to 2 V, and the olive dots are from the reverse situation; the inset is of the same curves in the semilogarithmic axis.

cross section at the fixed vertical coordinate, v_0 (the dashed white line in Figure 2(e)), reveals spectral dependence of the s-SNOM heterostructure nanotube contrasts as shown in Figure 2(f). The frequency dependence of amplitude normalized to the SiO₂ background, $S_2^{N}(f, x; y_0)$, shows negative contrast (absorption of the excitation light by the nanotube) in the whole spectral region except for a narrow band of positive contrast. This narrow band corresponds to the strongest phonon-polariton resonance of BNNT,34 which happens at a frequency of 1370 cm⁻¹ and is consistent with the Fourier transform IR (FTIR) measurement in previous reports. 31,35 The IR active mode of MoS₂NT is out of the examining range for BNNT. Instead, AES mapping of the post-transferred heterostructure nanotube resolved the difficulty of capturing signals from the three materials at the same time, and the results are presented in Figure S8.

Figure 3 exhibits the first diode device we discuss in this work. The SEM image in Figure 3(a) shows the nanotube before metal contact deposition, and the striking contrasts indicate that the bottom part of the nanotube is thicker than the upper part. Thereupon, the designed metal contacts, which were sputtered with 2 nm Cr and 20 nm Pd into the patterned trenches, are in touch with these two obviously different parts of the nanotube and denoted as electrodes E1 and E2, respectively, as shown in Figure 3(b). Atomic force microscope (AFM) mapping in Figure 3(c) confirms the previous interpretation and assumption that the contrast appearance along nanotube in SEM images is indeed reflecting the thickness of the nanotube. The height profiles on the two electrodes are illustrated in Figure 3(d,e), quantifying the

bottom part of the nanotube as thick as 11 nm, while the upper part is as thin as only 1.4 nm, which is a common diameter of an SWCNT from our CVD system.³⁶ Therefore, we can tentatively conclude that electrode E1 is in contact with MoS₂NT, while electrode E2 is attached to SWCNT.

Current-voltage (I-V) measurements were conducted on the heterostructure device, and a schematic cross-sectional view is depicted in Figure 4(a). When one electrode is grounded while the other is applied with a driving bias sweeping from -2 to 2 V, there is a strong rectifying effect no matter if the charge carriers were injected from either electrode. The noticeable difference from sweeping voltages on the two electrodes is the voltage polarity of the ON state. As shown in Figure 4(b), I-V curves from the two situations seem centrosymmetric, which is bespeaking a common source for the rectifying effect, but electrode E1 prefers a negative voltage polarity while electrode E2 prefers the opposite. To verify that the rectifying effect is originated from the S-I-S heterojunction but not from the metal-semiconductor interface, namely, the Schottky barrier, a normal SWCNT device with the same configuration on the same target chip and transferred from the same as-grown substrate is comparatively analyzed alongside the heterostructure device as a reference, and it is presented in Figure S9. First of all, unlike the unevenness of the heterostructure shown in Figure 3, the referential SWCNT device shows a uniform surface in SEM as can be found in Figure S9(a,b) before and after metal deposition, respectively. The metal contacts in this work are basically Pd (Cr as an adhesive layer and its thickness of 2 nm are not enough to form an intact thin film), which is believed

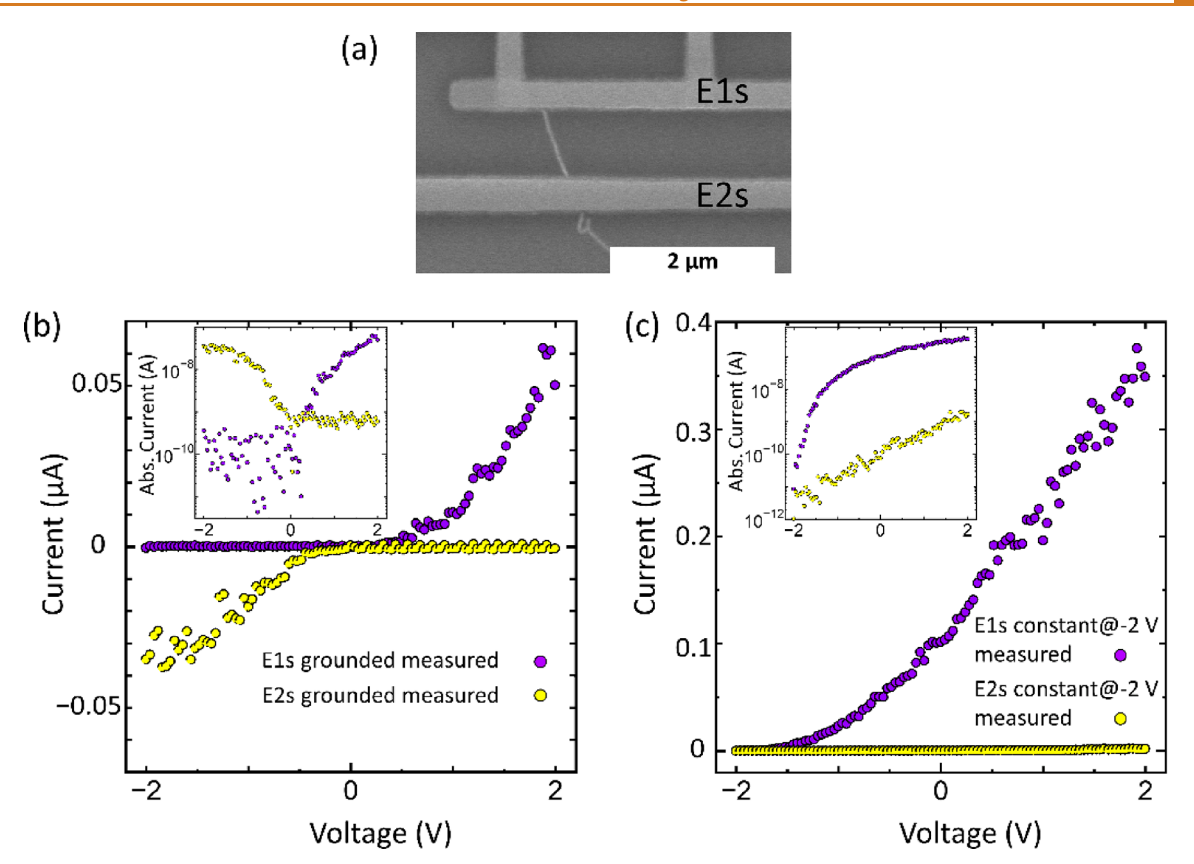


Figure 5. (a) SEM image of the diode device. (b) Electrical characteristics: the purple dots are measured when electrode E1s (denoted in (a)) is grounded while electrode E2s is sweeping from -2 to 2 V, and the yellow dots are from the reverse situation; the inset shows the same curves in the semilogarithmic axis. (c) Electrical characteristics: the purple dots are measured when electrode E1s is at a constant of -2 V while electrode E2s is sweeping from -2 to 2 V, and the yellow dots are from the reverse situation; the inset is of the same curves in the semilogarithmic axis.

to provide Ohmic contacts for hole injections to CNT, 23 while in reality, the contact resistance is impeding the smooth transfer of charge carriers, as shown in Figure S9(c). Electrode E2r is end-bonded with the SWCNT and has a larger contact area in comparison with the side-bonded electrode E1r, so the resistance is much smaller when the charge carriers are introduced from electrode E2r, as reflected by the I-V curves in Figure S9(c). Although the contact condition has a strong influence on the I-V curves, the rectifying effect deriving from the Schottky barrier between the metal and semiconducting SWCNT is allowing hole injection and hindering electron injection from both electrodes. For the Schottky barrier between MoS₂ and Pd, a similar behavior can be anticipated. Consequently, we can exclude the Schottky barrier as the main origin of the rectifying effect from the heterostructure device in Figure 4, and there leaves no other factor but the S-I-S heterojunction to account for the effect. The I-V curves in the range from -1 to 1 V of Figure 4(b) were also finely fitted by a modified diode equation³⁷ expressed as

$$I = I_{s}(e^{q(V-I\cdot R_{s})/nk_{B}T} - 1) + \frac{V}{R_{sh}}$$
(1)

in which n, q, $k_{\rm B}$, and T are constants of the ideality factor (n=1.2), 17 electron charge, Boltzmann constant, and absolute temperature, respectively. $I_{\rm s}$, $R_{\rm s}$, and $R_{\rm sh}$ are fitting parameters of the dark saturation current, series resistance, and shunt resistance, respectively. Details of the fitting parameters can be found in Table S1.

As analyzed before and illustrated in Figure 4(a), electrode E1 is in contact with MoS_2NT , which is expressing as an *n*-type semiconductor due to natural doping, although it is linked to high work function metal such as Pd, as a result of strong Fermi level pinning;³⁸ and electrode E2 is covering the SWCNT, which shows p-type semiconductor characteristics.³⁹ Therefore, we can expect that a negative voltage polarity on electrode E1 and a positive voltage polarity on electrode E2 will supply a forward bias for this S-I-S heterojunction diode, while the reverse scenario will block the flow of current. In Figure 4(c), one electrode of the heterostructure was applied with a constant voltage of -2 V, while the other was driven by a sweeping voltage from -2 to 2 V. With the forward bias, the current is rapidly increasing with the voltage drop, while the reverse bias results in a much lower current. With a bias drop of 4 V, therectification ratio is 24, outperforming the previously reported 2D S-I-S diode. 20 On the other side, if a 2D S-I-S diode is as narrow as the 1D heterojunction diode presented here, it will result in degradation of the conductance due to disordered edges and will be inadaptable to the need of highresolution and high-sensitivity photodetectors. Additionally, the same measurements were also performed on the referential SWCNT device as shown in Figure S9(d). Because both electrodes were biased in these measurements, the effect of the voltage barrier caused by contact resistance is indistinguishable no matter which electrode is constantly negatively biased while the driving bias on the other electrode is sweeping. Therefore, I-V curves are almost identical when the status of bias is switched between the two contact electrodes. Moreover, as was

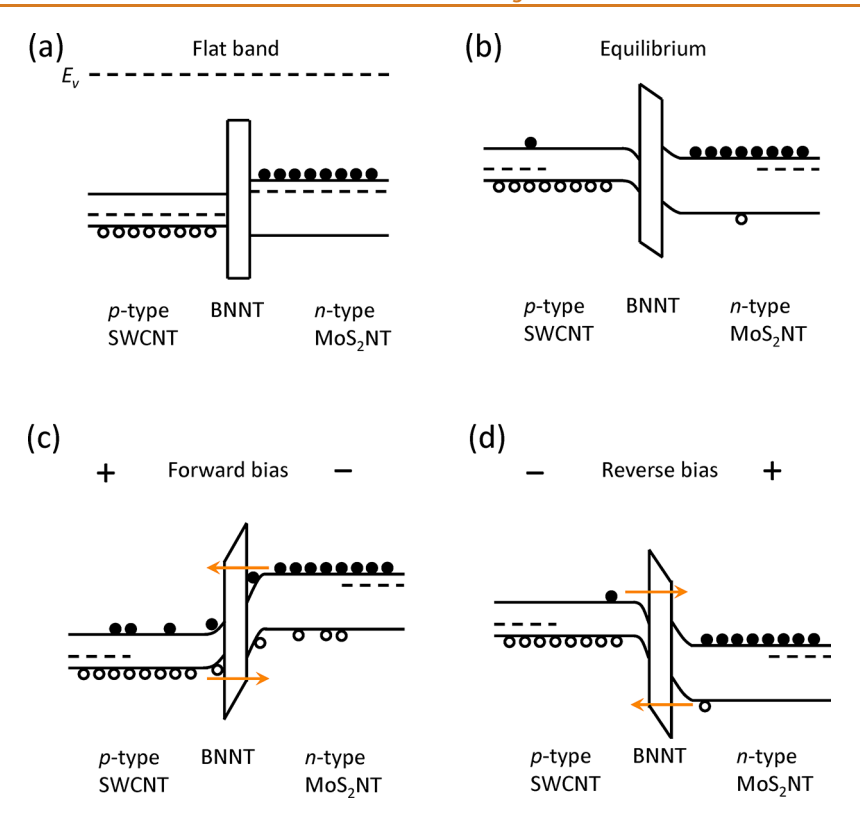


Figure 6. Schematics of the energy band diagram of the 1D S-I-S heterojunction diode: (a) flat band, (b) equilibrium, (c) forward bias, and (d) reverse bias.

compared in ref 20, the existence of insulating BNNT is of crucial importance to guarantee the tunneling transport of charge carriers that leads to a higher current and improved rectification ratio. The ON current density of the diode device in Figure 4 is shown in Figure S10, which is comparable to that in 2D BN tunneling devices. We also observed an improved rectification ratio from a follow-up heterostructure nanotube device over 10³ with a driving bias of 2 V, and the diode characteristics are presented in Figure 5. The current carrying capability is closely related to the band gap of SWCNT channel; therefore, it is impractical to evaluate this figure of merit by comparing the present S–I–S heterojunction diode and normal SWCNT device.

The carrier transport mechanism of the S-I-S heterojunction diode is explained in schematics of the energy band diagram illustrated in Figure 6. The band gap of SWCNT is determined by its chirality. 41 As the measured diameter is around 1.4 nm, the chiralities with a close diameter possess a band gap around 1.0 eV. 42 Moreover, the band gap of BNNT is referenced as to be 5.5 eV,43 and we measured the photoluminescence (PL) signal from the suspended heterostructure nanotube to be 1.88 eV as shown in Figure S11, close to the previous reports about 2D MoS₂, 44,45 so we assigned the contribution of the emerging PL signal to be from MoS₂NT. The work function of the SWCNT is 5.05 eV,46 while the electron affinities of MoS2NT and BNNT are taken from the literature as 4.2⁴⁷ and 2 eV, 48 respectively. On the basis of these parameters, the flat band of the SWCNT/BNNT/ MoS₂NT sandwich structure is depicted in Figure 6(a). If the insulating BNNT is very thick, it will stop any carriers transporting, and the band diagram will remain flat as in Figure 6(a). Otherwise, little resistance is met by majority carriers from both sides with a very thin BNNT (monolayer for

instance) in between, and an equilibrium status can be reached with the small band bending on the edge, exerting a small builtin potential radially on the enveloped thick heterostructure nanotube as shown in Figure 6(b). Also, the built-in potential will slightly deplete the inner SWCNT, while outside the coaxial structure, the exposed SWCNT is still intrinsically pdoped, which will make for an electrostatic potential laterally along the SWCNT, i.e., a lateral p^--p junction in series with a radial S-I-S heterojunction. When a forward bias is executed on the heterostructure device, which refers to a positive polarity on the SWCNT side while there is negative polarity on MoS_2NT side, as demonstrated in Figure 6(c), majority carriers from both sides of insulator are rapidly accumulating at the interface driven by potential and flattening the initial band bending (if there is) with an increase of the bias; the accumulated carriers swiftly tunnel through the insulting layer and lead to a raising current. On the other hand, a reverse bias will build up a high potential barrier to immobilize majority carriers, and minority carriers can only provide a small current flow as schematically illustrated in Figure 6(d). This tunneling mechanism provides explanation for the rectifying effect measured in Figures 4/5, and the aforementioned lateral $p^$ p junction in series will additionally contribute to the overall rectifying effect. Furthermore, comparing the I-V curves of the heterojunction diode (in Figures 4/5) and the normal SWCNT device (in Figure S9), we can conclude that the metal contact effect is negligible to the overall performance of the diode, considering that the condition of the two contacts are very different in the heterojunction diode, but no noticeable influence is present when the driving bias switches from one electrode to the other.

To further elucidate the underlying working mechanism of the S-I-S heterojunction diode, we performed field effect

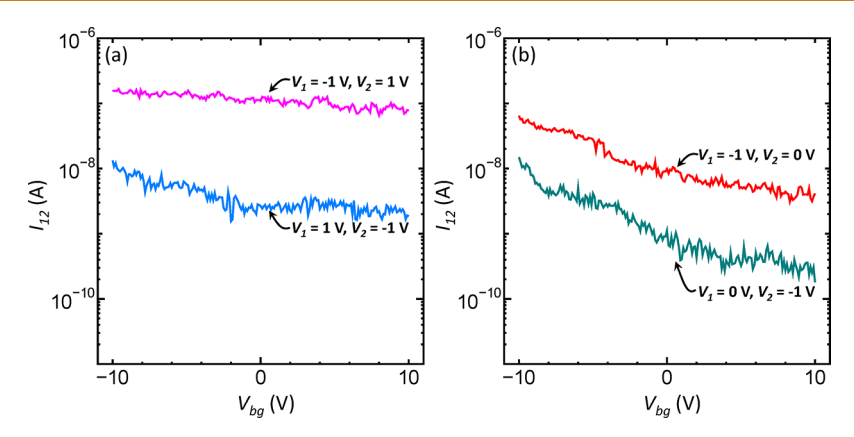


Figure 7. Channel current as a function of back-gate voltages: (a) the magenta solid line is when the applied voltage on electrode E1 is -1 V and that on electrode E2 is 1 V; the blue solid line is when the applied voltage on electrode E1 is 1 V and that on electrode E2 is -1 V. (b) The red solid line is when the applied voltage on electrode E1 is -1 V and that on electrode E2 is 0 V; the olive solid line is when the applied voltage on electrode E1 is -1 V.

measurements on the former device (Figure 4) as shown in Figure 7. When electrode E1 was supplied with a constant voltage of -1 V and electrode E2 was supplied with 1 V, it was the ON state of the diode, and the current flow between the two electrodes was barely affected by the back-gating on silicon, which was sweeping from -10 to 10 V, as the magenta solid curve in Figure 7(a) demonstrates. On the other hand, when the device was under the OFF state, which was experiencing a reverse bias with electrode E1 of 1 V and electrode E2 of -1 V, the current was more than 1 magnitude lower than the ON current, as the blue solid curve in Figure 7(a) shows, and it starts decreasing slightly with the gating voltage, rendering an improved rectification ratio. This is analogous to the transfer characteristics of the CNT Schottky diode enabled by asymmetric metal contacts.⁴⁹ Reducing the driving bias on the diode from 2 to 1 V by decreasing the voltage on electrode E2 from 1 to 0 V, as shown in Figure 7(b), the ON current was rapidly dropping, and the field effect was starting to play a role to tune the ON current as the changes from the magenta solid curve to red solid curve imply. The OFF current was experiencing similar changes when the voltage on electrode E1 decreased from 1 to 0 V, but the current drop was smaller than that of the ON current. A negative back-gate bias (less than 10 V, see Figure S12) could turn the Schottky contact between Pd and SWCNT into an Ohmic contact. Respectively, to turn the Schottky contact between Pd and MoS₂ into an Ohmic contact, a relatively larger back-gate bias is needed.³⁸ This is to say the Schottky barrier between Pd and MoS₂ is higher than that between Pd and SWCNT, and for the two back-to-back Schottky barriers, a slight advantage should be for a negative back-gate bias. In agreement, it can be noticed that the devices are more sensitive to the gate bias for a smaller forward/reverse bias that leads to less drive force for carriers to penetrate the barriers, as demonstrated in Figure 7. On the other hand, the back-gate bias has an indistinguishable influence on the rectification ratio of the diode, which is more proof that the rectifying effect has little to do with the Schottky junctions. Although the performance of *n*-type MoS₂ transistor⁵⁰ was not as good as the p-type SWCNT transistor⁵¹ with regard to a unified geometry because of a much lower carrier mobility, the fieldunaffected ON current presented here indicating a competition from both factors that offset the gating effect so that the functionality of MoS₂NT in the present work was comparable

to SWCNT to some extent. Therefore, apart from the tremendous potentialities exhibited by the current 1D S–I–S heterostructure diode in applications such as a photodetector and solar cells, after the inner SWCNT is removed, the MoS_2NT can be a very promising candidate for the next generation electronics or optoelectronics with a steady large bandgap regardless of the chirality. As a good comparison, the transfer characteristics of the normal SWCNT device are presented in Figure S12.

CONCLUSIONS

A µm-long coaxial van der Waals heterostructure nanotube composed of an SWCNT, BNNT, and MoS2NT has been synthesized. An S-I-S architecture can be identified given the template SWCNT is semiconducting. Without any intentional interference, semiconducting SWCNT demonstrates p-type characteristics with conventional noble metal contacts, while MoS₂NT behaves like an *n*-type semiconductor. On account of these, we are presenting an S-I-S heterojunction radially, which results in an SWCNT-BNNT-MoS2NT diode as narrow as 11 nm. The heterojunction diode demonstrates a rectification ratio of 24 with a bias voltage of 4 V, which is outperforming a similar 2D heterojunction diode. In addition, an improved rectification ratio over 10³ was observed. The insulating BNNT is of crucial importance that not only facilitates the wrapping of MoS2NT and also provides tunneling media that influences the ON and OFF current of diode as well as its rectification ratio, so a precise control growth of the heterostructure layers will benefit the performance of such heterostructure devices.

METHODS

Fabrication Processes. Electron beam lithography (EBL) was utilized to make mark and frame patterns, and then, the patterns were transferred onto a 525- μ m-thick Si substrate (100 nm SiO₂ on the top) by reactive ion etching (RIE), removing about 200 nm of the top layer. Co catalysts (0.3 nm) were deposited by sputtering in EBL patterned areas. Catalyst areas were protected by a resist, and the exposed areas were etched by RIE and deep reactive ion etching (DRIE) to produce 8- μ m-high Si poles. SWCNTs were synthesized by bridging Si poles by alcohol catalytic chemical vapor deposition (ACCVD), during which alcohol as a carbon source was introduced for 10 min at 800 °C. BNNT coating was performed with 30 mg of ammonia borane (H₃NBH₃) as a precursor at the upstream and heated to 70 °C and a sample furnace at 1075 °C for 2 h. MoS₂NT

coating was followed with sulfur (S) powder at the upstream and heated to 138 $^{\circ}$ C, while molybdenum oxide (MoO₃) and a sample chip were kept 8 cm apart in the furnace at 530 $^{\circ}$ C for 50 min. The asgrown 1D heterostructure nanotubes were face-transferred onto a target chip assisted by water vapor. Electrical connections were patterned by EBL and realized by sputtering 2 nm chromium (Cr) plus 20 nm palladium (Pd) as metal contacts.

Characterization of Heterostructure Nanotubes. Raman and PL spectra were taken by a Raman spectrometer (inVia, Renishaw) with the excitation wavelength of 532 nm. An AES spectrum was obtained through FE-Auger Electron Spectroscopy Model SAM-680. The hyperspectral imaging of heterostructure nanotubes was performed using a customized neaSNOM microscope (Neaspec GmbH): AFM combined with a UV-vis-NIR-MIR excitation system and electronics. Electrical measurements were conducted in a back-gate geometry in air at room temperature using a semiconductor parameter analyzer (Agilent, 4156C).

ASSOCIATED CONTENT

Supporting Information

The Supporting Information is available free of charge at https://pubs.acs.org/doi/10.1021/acsnano.1c00657.

Schematics of fabrication processes, material preparations, and face-transfer techniques, SEM images of asgrown and transferred heterostructure nanotubes, full Raman spectrum of suspended heterostructure nanotube, s-SNOM scan images at 26 different IR frequencies, AES mapping of post-transferred heterostructure nanotubes, current density of the diode device, electrical measurements of the referential SWCNT device, and PL of the suspended heterostructure nanotube (PDF)

AUTHOR INFORMATION

Corresponding Authors

Shigeo Maruyama — Department of Mechanical Engineering, School of Engineering, The University of Tokyo, Tokyo 113-8656, Japan; oorcid.org/0000-0003-3694-3070; Email: maruyama@photon.t.u-tokyo.ac.jp

Ya Feng — Department of Mechanical Engineering, School of Engineering, The University of Tokyo, Tokyo 113-8656, Japan; orcid.org/0000-0003-3049-9933; Email: fengya@photon.t.u-tokyo.ac.jp

Authors

Henan Li – Department of Mechanical Engineering, School of Engineering, The University of Tokyo, Tokyo 113-8656, Iapan

Taiki Inoue — Department of Mechanical Engineering, School of Engineering, The University of Tokyo, Tokyo 113-8656, Japan; Department of Applied Physics, Graduate School of Engineering, Osaka University, Osaka 565-0871, Japan; orcid.org/0000-0003-1739-917X

Shohei Chiashi — Department of Mechanical Engineering, School of Engineering, The University of Tokyo, Tokyo 113-8656, Japan; © orcid.org/0000-0002-3813-0041

Slava V. Rotkin — Department of Engineering Science and Mechanics, Materials Research Institute, The Pennsylvania State University, Millennium Science Complex, University Park, Pennsylvania 16802, United States

Rong Xiang — Department of Mechanical Engineering, School of Engineering, The University of Tokyo, Tokyo 113-8656, Japan; occid.org/0000-0002-4775-4948

Complete contact information is available at:

https://pubs.acs.org/10.1021/acsnano.1c00657

Author Contributions

Y.F. and S.M. conceived the project. Y.F. and T.I. developed the device fabrication scheme. Y.F. fabricated the silicon-pole chip and synthesized SWCNTs. H.L. conducted BNNT and MoS₂NT coating. Y.F. transferred as-grown heterostructure nanotubes and designed the diode structure. Y.F. characterized samples by SEM, Raman (PL), and AES. S.V.R. performed s-SNOM measurements. Y.F. took electrical measurements. Y.F., S.V.R., and S.M. analyzed the data. Y.F. wrote the manuscript. All the authors participated in the discussion of the work and commented on the manuscript.

Notes

The authors declare no competing financial interest.

ACKNOWLEDGMENTS

Part of this work was supported by JSPS KAKENHI (grant numbers JP18H05329, JP19H02543, JP20H00220, and JP20KK0114) and by JST, CREST Grant Number JPMJCR20B5, Japan. The work of S.V.R. was supported by the National Science Foundation (Grant DMR-2011839). Part of this work was conducted at the Takeda Sentanchi Supercleanroom, supported by the "Nanotechnology Platform" of the Ministry of Education, Culture, Sports, Science and Technology (MEXT), Japan, Grant number JPMXP09F19UT0006.

REFERENCES

- (1) Sze, S. M.; Ng, K. K. Physics of Semiconductor Devices, 3rd ed.; John Wiley & Sons, Inc.: Hoboken, NJ, 2006.
- (2) Geim, A. K.; Grigorieva, I. V. Van der Waals Heterostructures. *Nature* **2013**, 499, 419.
- (3) Liu, Y.; Weiss, N. O.; Duan, X.; Cheng, H.-C.; Huang, Y.; Duan, X. Van der Waals Heterostructures and Devices. *Nature Reviews Materials* **2016**, *1*, 16042.
- (4) Lin, Y.-C.; Ghosh, R. K.; Addou, R.; Lu, N.; Eichfeld, S. M.; Zhu, H.; Li, M.-Y.; Peng, X.; Kim, M. J.; Li, L.-J.; Wallace, R. M.; Datta, S.; Robinson, J. A. Atomically Thin Resonant Tunnel Diodes Built from Synthetic van der Waals Heterostructures. *Nat. Commun.* **2015**, *6* (1), 7311
- (5) Sarkar, D.; Xie, X.; Liu, W.; Cao, W.; Kang, J.; Gong, Y.; Kraemer, S.; Ajayan, P. M.; Banerjee, K. A Subthermionic Tunnel Field-Effect Transistor with an Atomically Thin Channel. *Nature* **2015**, 526 (7571), 91–95.
- (6) Chu, D.; Lee, Y. H.; Kim, E. K. Selective Control of Electron and Hole Tunneling in 2D Assembly. *Science Advances* **2017**, 3 (4), No. e1602726.
- (7) Li, H.-M.; Lee, D.-Y.; Choi, M. S.; Qu, D.; Liu, X.; Ra, C.-H.; Yoo, W. J. Metal-Semiconductor Barrier Modulation for High Photoresponse in Transition Metal Dichalcogenide Field Effect Transistors. *Sci. Rep.* **2015**, *4* (1), 4041.
- (8) Lee, C.-H.; Lee, G.-H.; van der Zande, A. M.; Chen, W.; Li, Y.; Han, M.; Cui, X.; Arefe, G.; Nuckolls, C.; Heinz, T. F.; Guo, J.; Hone, J.; Kim, P. Atomically Thin *p-n* Junctions with van der Waals Heterointerfaces. *Nat. Nanotechnol.* **2014**, *9* (9), 676–681.
- (9) Withers, F.; Del Pozo-Zamudio, O.; Mishchenko, A.; Rooney, A. P.; Gholinia, A.; Watanabe, K.; Taniguchi, T.; Haigh, S. J.; Geim, A. K.; Tartakovskii, A. I.; Novoselov, K. S. Light-Emitting Diodes by Band-Structure Engineering in van der Waals Heterostructures. *Nat. Mater.* **2015**, *14* (3), 301–306.
- (10) Pyatkov, F.; Fütterling, V.; Khasminskaya, S.; Flavel, B. S.; Hennrich, F.; Kappes, M. M.; Krupke, R.; Pernice, W. H. P. Cavity-Enhanced Light Emission from Electrically Driven Carbon Nanotubes. *Nat. Photonics* **2016**, *10*, 420.

- (11) Qiu, C.; Zhang, Z.; Xiao, M.; Yang, Y.; Zhong, D.; Peng, L.-M. Scaling Carbon Nanotube Complementary Transistors to 5-nm Gate Lengths. *Science* **2017**, *355* (6322), 271–276.
- (12) Graf, A.; Held, M.; Zakharko, Y.; Tropf, L.; Gather, M. C.; Zaumseil, J. Electrical Pumping and Tuning of Exciton-Polaritons in Carbon Nanotube Microcavities. *Nat. Mater.* **2017**, *16*, 911.
- (13) Cui, K.; Anisimov, A. S.; Chiba, T.; Fujii, S.; Kataura, H.; Nasibulin, A. G.; Chiashi, S.; Kauppinen, E. I.; Maruyama, S. Air-Stable High-Efficiency Solar Cells with Dry-Transferred Single-Walled Carbon Nanotube Films. *J. Mater. Chem. A* **2014**, *2* (29), 11311–11318.
- (14) Zhou, C.; Kong, J.; Yenilmez, E.; Dai, H. Modulated Chemical Doping of Individual Carbon Nanotubes. *Science* **2000**, 290 (5496), 1552–1555.
- (15) Kang, B. R.; Yu, W. J.; Kim, K. K.; Park, H. K.; Kim, S. M.; Park, Y.; Kim, G.; Shin, H.-J.; Kim, U. J.; Lee, E.-H.; Choi, J.-Y.; Lee, Y. H. Restorable Type Conversion of Carbon Nanotube Transistor Using Pyrolytically Controlled Antioxidizing Photosynthesis Coenzyme. *Adv. Funct. Mater.* **2009**, *19* (16), 2553–2559.
- (16) Peng, L.-M.; Zhang, Z.; Wang, S.; Liang, X. A Doping-Free Approach to Carbon Nanotube Electronics and Optoelectronics. *AIP Adv.* **2012**, 2 (4), No. 041403.
- (17) Lee, J. U.; Gipp, P. P.; Heller, C. M. Carbon Nanotube *p-n* Junction Diodes. *Appl. Phys. Lett.* **2004**, *85* (1), 145–147.
- (18) Mueller, T.; Kinoshita, M.; Steiner, M.; Perebeinos, V.; Bol, A. A.; Farmer, D. B.; Avouris, P. Efficient Narrow-Band Light Emission from a Single Carbon Nanotube *p-n* Diode. *Nat. Nanotechnol.* **2010**, *5*, 27.
- (19) Gupta, G.; Rajasekharan, B.; Hueting, R. J. E. Electrostatic Doping in Semiconductor Devices. *IEEE Trans. Electron Devices* **2017**, 64 (8), 3044–3055.
- (20) Jeong, H.; Bang, S.; Oh, H. M.; Jeong, H. J.; An, S.-J.; Han, G. H.; Kim, H.; Kim, K. K.; Park, J. C.; Lee, Y. H.; Lerondel, G.; Jeong, M. S. Semiconductor-Insulator-Semiconductor Diode Consisting of Monolayer MoS₂, h-BN. ACS Nano **2015**, *9* (10), 10032–10038.
- (21) Wang, L.; Meric, I.; Huang, P.; Gao, Q.; Gao, Y.; Tran, H.; Taniguchi, T.; Watanabe, K.; Campos, L.; Muller, D.; et al. One-Dimensional Electrical Contact to a Two-Dimensional Material. *Science* **2013**, 342 (6158), 614–617.
- (22) Xiang, R.; Inoue, T.; Zheng, Y.; Kumamoto, A.; Qian, Y.; Sato, Y.; Liu, M.; Tang, D.; Gokhale, D.; Guo, J.; Hisama, K.; Yotsumoto, S.; Ogamoto, T.; Arai, H.; Kobayashi, Y.; Zhang, H.; Hou, B.; Anisimov, A.; Maruyama, M.; Miyata, Y.; et al. One-Dimensional van der Waals Heterostructures. *Science* **2020**, *367* (6477), 537.
- (23) Javey, A.; Guo, J.; Wang, Q.; Lundstrom, M.; Dai, H. Ballistic Carbon Nanotube Field-Effect Transistors. *Nature* **2003**, 424 (6949), 654–657.
- (24) Fathipour, S.; Remskar, M.; Varlec, A.; Ajoy, A.; Yan, R.; Vishwanath, S.; Rouvimov, S.; Hwang, W. S.; Xing, H. G.; Jena, D.; Seabaugh, A. Synthesized Multiwall MoS₂ Nanotube and Nanoribbon Field-Effect Transistors. *Appl. Phys. Lett.* **2015**, *106* (2), No. 022114.
- (25) Léonard, F.; Stewart, D. A. Properties of Short Channel Ballistic Carbon Nanotube Transistors with Ohmic Contacts. *Nanotechnology* **2006**, *17* (18), 4699–4705.
- (26) Franklin, A. D.; Koswatta, S. O.; Farmer, D. B.; Smith, J. T.; Gignac, L.; Breslin, C. M.; Han, S.-J.; Tulevski, G. S.; Miyazoe, H.; Haensch, W.; Tersoff, J. Carbon Nanotube Complementary Wrap-Gate Transistors. *Nano Lett.* **2013**, *13* (6), 2490–2495.
- (27) Chen, X.; Roemer, M.; Yuan, L.; Du, W.; Thompson, D.; del Barco, E.; Nijhuis, C. A. Molecular Diodes with Rectification Ratios Exceeding 10⁵ Driven by Electrostatic Interactions. *Nat. Nanotechnol.* **2017**, 12 (8), 797–803.
- (28) Capozzi, B.; Xia, J.; Adak, O.; Dell, E. J.; Liu, Z.-F.; Taylor, J. C.; Neaton, J. B.; Campos, L. M.; Venkataraman, L. Single-Molecule Diodes with High Rectification Ratios through Environmental Control. *Nat. Nanotechnol.* **2015**, *10* (6), 522–527.
- (29) Arai, H.; Inoue, T.; Xiang, R.; Maruyama, S.; Chiashi, S. Non-Catalytic Heteroepitaxial Growth of Aligned, Large-Sized Hexagonal

- Boron Nitride Single-Crystals on Graphite. Nanoscale 2020, 12 (18), 10399-10406.
- (30) Abrams, Z. e. R.; Ioffe, Z.; Tsukernik, A.; Cheshnovsky, O.; Hanein, Y. J. N. l. A Complete Scheme for Creating Predefined Networks of Individual Carbon Nanotubes. *Nano Lett.* **2007**, *7* (9), 2666–2671.
- (31) Dai, S.; Fei, Z.; Ma, Q.; Rodin, A. S.; Wagner, M.; McLeod, A. S.; Liu, M. K.; Gannett, W.; Regan, W.; Watanabe, K.; Taniguchi, T.; Thiemens, M.; Dominguez, G.; Neto, A. H. C.; Zettl, A.; Keilmann, F.; Jarillo-Herrero, P.; Fogler, M. M.; Basov, D. N. Tunable Phonon Polaritons in Atomically Thin van der Waals Crystals of Boron Nitride. *Science* **2014**, *343* (6175), 1125–1129.
- (32) Woessner, A.; Lundeberg, M. B.; Gao, Y.; Principi, A.; Alonso-González, P.; Carrega, M.; Watanabe, K.; Taniguchi, T.; Vignale, G.; Polini, M.; Hone, J.; Hillenbrand, R.; Koppens, F. H. L. Highly Confined Low-Loss Plasmons in Graphene-Boron Nitride Heterostructures. *Nat. Mater.* **2015**, *14* (4), 421–425.
- (33) Dai, S.; Quan, J.; Hu, G.; Qiu, C.-W.; Tao, T. H.; Li, X.; Alù, A. Hyperbolic Phonon Polaritons in Suspended Hexagonal Boron Nitride. *Nano Lett.* **2019**, *19* (2), 1009–1014.
- (34) Xu, X. G.; Ghamsari, B. G.; Jiang, J.-H.; Gilburd, L.; Andreev, G. O.; Zhi, C.; Bando, Y.; Golberg, D.; Berini, P.; Walker, G. C. One-Dimensional Surface Phonon Polaritons in Boron Nitride Nanotubes. *Nat. Commun.* **2014**, *5* (1), 4782.
- (35) Wang, P.; Zheng, Y.; Inoue, T.; Xiang, R.; Shawky, A.; Watanabe, M.; Anisimov, A.; Kauppinen, E. I.; Chiashi, S.; Maruyama, S. Enhanced In-Plane Thermal Conductance of Thin Films Composed of Coaxially Combined Single-Walled Carbon Nanotubes and Boron Nitride Nanotubes. ACS Nano 2020, 14 (4), 4298–4305.
- (36) Feng, Y.; Inoue, T.; An, H.; Xiang, R.; Chiashi, S.; Maruyama, S. Quantitative Study of Bundle Size Effect on Thermal Conductivity of Single-Walled Carbon Nanotubes. *Appl. Phys. Lett.* **2018**, *112* (19), 191904.
- (37) Ho, X.; Ye, L.; Rotkin, S. V.; Xie, X.; Du, F.; Dunham, S.; Zaumseil, J.; Rogers, J. A. Theoretical and Experimental Studies of Schottky Diodes that Use Aligned Arrays of Single-Walled Carbon Nanotubes. *Nano Res.* **2010**, 3 (6), 444–451.
- (38) Kim, C.; Moon, I.; Lee, D.; Choi, M. S.; Ahmed, F.; Nam, S.; Cho, Y.; Shin, H.-J.; Park, S.; Yoo, W. J. Fermi Level Pinning at Electrical Metal Contacts of Monolayer Molybdenum Dichalcogenides. *ACS Nano* **2017**, *11* (2), 1588–1596.
- (39) Franklin, A. D.; Farmer, D. B.; Haensch, W. Defining and Overcoming the Contact Resistance Challenge in Scaled Carbon Nanotube Transistors. *ACS Nano* **2014**, *8* (7), 7333–7339.
- (40) Britnell, L.; Gorbachev, R. V.; Jalil, R.; Belle, B. D.; Schedin, F.; Katsnelson, M. I.; Eaves, L.; Morozov, S. V.; Mayorov, A. S.; Peres, N. M. R.; Castro Neto, A. H.; Leist, J.; Geim, A. K.; Ponomarenko, L. A.; Novoselov, K. S. Electron Tunneling through Ultrathin Boron Nitride Crystalline Barriers. *Nano Lett.* **2012**, *12* (3), 1707–1710.
- (41) Dresselhaus, M.; Eklund, P. Phonons in Carbon Nanotubes. *Adv. Phys.* **2000**, 49 (6), 705–814.
- (42) Dukovic, G.; Wang, F.; Song, D.; Sfeir, M. Y.; Heinz, T. F.; Brus, L. E. Structural Dependence of Excitonic Optical Transitions and Band-Gap Energies in Carbon Nanotubes. *Nano Lett.* **2005**, *5* (11), 2314–2318.
- (43) Jaffrennou, P.; Barjon, J.; Lauret, J.-S.; Maguer, A.; Golberg, D.; Attal-Trétout, B.; Ducastelle, F.; Loiseau, A. Optical Properties of Multiwall Boron Nitride Nanotubes. *Phys. Status Solidi B* **2007**, 244 (11), 4147–4151.
- (44) Splendiani, A.; Sun, L.; Zhang, Y.; Li, T.; Kim, J.; Chim, C.-Y.; Galli, G.; Wang, F. Emerging Photoluminescence in Monolayer MoS₂. *Nano Lett.* **2010**, *10* (4), 1271–1275.
- (45) Sup Choi, M.; Lee, G.-H.; Yu, Y.-J.; Lee, D.-Y.; Hwan Lee, S.; Kim, P.; Hone, J.; Jong Yoo, W. Controlled Charge Trapping by Molybdenum Disulphide and Graphene in Ultrathin Heterostructured Memory Devices. *Nat. Commun.* **2013**, *4* (1), 1624.
- (46) Shiraishi, M.; Ata, M. Work Function of Carbon Nanotubes. *Carbon* **2001**, *39* (12), 1913–1917.

- (47) Schlaf, R.; Lang, O.; Pettenkofer, C.; Jaegermann, W. Band Lineup of Layered Semiconductor Heterointerfaces Prepared by van der Waals Epitaxy: Charge Transfer Correction Term for the Electron Affinity Rule. *J. Appl. Phys.* **1999**, *85* (5), 2732–2753.
- (48) Cumings, J.; Zettl, A. Field Emission and Current-Voltage Properties of Boron Nitride Nanotubes. *Solid State Commun.* **2004**, 129 (10), 661–664.
- (49) Yang, M. H.; Teo, K. B. K.; Milne, W. I.; Hasko, D. G. Carbon Nanotube Schottky Diode and Directionally Dependent Field-Effect Transistor Using Asymmetrical Contacts. *Appl. Phys. Lett.* **2005**, 87 (25), 253116.
- (50) Radisavljevic, B.; Radenovic, A.; Brivio, J.; Giacometti, V.; Kis, A. Single-Layer MoS₂ Transistors. *Nat. Nanotechnol.* **2011**, *6* (3), 147–150.
- (51) Franklin, A. D.; Luisier, M.; Han, S.-J.; Tulevski, G.; Breslin, C. M.; Gignac, L.; Lundstrom, M. S.; Haensch, W. J. N. l. Sub-10 nm Carbon Nanotube Transistor. *Nano Lett.* **2012**, *12* (2), 758–762.